

Unveiling light collection and pump enhancement from quantum wells with plasmonic metasurfaces using power dependent measurements

Citation for published version (APA):

Abdelkhalik, M. S., Vaskin, A., López, T., Abass, A., & Gómez Rivas, J. (2023). Unveiling light collection and pump enhancement from quantum wells with plasmonic metasurfaces using power dependent measurements. *JPhys Photonics*, 5(2), Article 025001. <https://doi.org/10.1088/2515-7647/acc7e6>

Document license:
CC BY

DOI:
[10.1088/2515-7647/acc7e6](https://doi.org/10.1088/2515-7647/acc7e6)

Document status and date:
Published: 01/04/2023

Document Version:
Publisher's PDF, also known as Version of Record (includes final page, issue and volume numbers)

Please check the document version of this publication:

- A submitted manuscript is the version of the article upon submission and before peer-review. There can be important differences between the submitted version and the official published version of record. People interested in the research are advised to contact the author for the final version of the publication, or visit the DOI to the publisher's website.
- The final author version and the galley proof are versions of the publication after peer review.
- The final published version features the final layout of the paper including the volume, issue and page numbers.

[Link to publication](#)

General rights

Copyright and moral rights for the publications made accessible in the public portal are retained by the authors and/or other copyright owners and it is a condition of accessing publications that users recognise and abide by the legal requirements associated with these rights.

- Users may download and print one copy of any publication from the public portal for the purpose of private study or research.
- You may not further distribute the material or use it for any profit-making activity or commercial gain
- You may freely distribute the URL identifying the publication in the public portal.

If the publication is distributed under the terms of Article 25fa of the Dutch Copyright Act, indicated by the "Taverne" license above, please follow below link for the End User Agreement:

www.tue.nl/taverne

Take down policy

If you believe that this document breaches copyright please contact us at:

openaccess@tue.nl

providing details and we will investigate your claim.

PAPER • OPEN ACCESS

Unveiling light collection and pump enhancement from quantum wells with plasmonic metasurfaces using power dependent measurements

To cite this article: Mohamed S Abdelkhalik *et al* 2023 *J. Phys. Photonics* **5** 025001

View the [article online](#) for updates and enhancements.

You may also like

- [Active optical metasurfaces: comprehensive review on physics, mechanisms, and prospective applications](#)
Jingyi Yang, Sudip Gurung, Subhajit Bej et al.
- [Metasurfaces: a new look at Maxwell's equations and new ways to control light](#)
M A Remnev and V V Klimov
- [Resonant dielectric metasurfaces: active tuning and nonlinear effects](#)
Chengjun Zou, Jürgen Sautter, Frank Setzpfandt et al.



PAPER

OPEN ACCESS

RECEIVED
4 January 2023REVISED
9 March 2023ACCEPTED FOR PUBLICATION
27 March 2023PUBLISHED
11 April 2023

Original Content from
this work may be used
under the terms of the
[Creative Commons
Attribution 4.0 licence](#).

Any further distribution
of this work must
maintain attribution to
the author(s) and the title
of the work, journal
citation and DOI.



Unveiling light collection and pump enhancement from quantum wells with plasmonic metasurfaces using power dependent measurements

Mohamed S Abdelkhalik^{1,*} , Aleksandr Vaskin¹, Toni López², Aimi Abass² and Jaime Gómez Rivas¹¹ Department of Applied Physics and Science Education, and Eindhoven Hendrik Casimir Institute, PO Box 513, Eindhoven, 5600 MB, The Netherlands² Lumileds Germany GmbH, D-52068 Aachen, Germany

* Author to whom any correspondence should be addressed.

E-mail: m.m.s.abdelkhalik.mohamed@tue.nl**Keywords:** metasurfaces, LEDs, light collection enhancement, numerical simulationsSupplementary material for this article is available [online](#)

Abstract

Low light extraction efficiency (LEE) is the greatest limiting factor for the brightness of reduced-size light-emitting diodes (LEDs) as it limits their emission intensity. In addition, LEDs have a Lambertian emission, which requires secondary optics to control the emission directionality. Plasmonic metasurfaces can introduce a way of manipulating the generated light from LEDs to enhance their LEE and steer the emitted light by reshaping the far-field emission. Here, we fabricate resonant plasmonic metasurfaces on top of a typical blue emitting wafer consisting of InGaN/gallium nitride quantum wells developed for commercial LED devices. The metasurface is separated from the InGaN quantum wells by p-GaN and indium-tin-oxide (ITO) layers with a cumulative thickness of 110 nm. Since this distance value is close to the emission wavelength in the corresponding medium, enhanced near-fields of localized plasmonic resonances do not reach the active region. Despite this, we observe a strong influence of the metasurfaces on the far-field photoluminescence emission from the quantum wells as demonstrated by Fourier imaging. Power-dependent excitation measurements of the samples allow us to retrieve the pump and light collection enhancement factors provided by the plasmonic metasurfaces. We demonstrate that the plasmonic metasurfaces can provide a pump enhancement factor of up to 4.1 and a collection enhancement factor of up to 3.2. We have also performed simulations based on the reciprocity principle and achieved a good qualitative agreement with the experimental results.

1. Introduction

Blue light-emitting diodes (LEDs) based on gallium nitride (GaN) have numerous applications in fields such as energy-efficient illumination, displays, augmented and virtual reality [1–5]. However, mini/micro GaN-based LEDs suffer from low light extraction efficiency (LEE) caused by the high-refractive index contrast between GaN and air. Therefore, a large fraction of the generated light is trapped within the device by total internal reflection for angles of emission larger than the critical angle (θ_c) [6, 7]. The outcoupling of this emission is a challenging task that limits the emission intensity [8, 9]. Rough walls on LED substrates sapphire allow for increasing the outcoupling efficiency. However, making walls rough is not compatible with micro-LEDs, which have compact and small sizes. The emission of typical GaN LED is Lambertian with no directional control of this emission over angle. LEDs require additional optical elements for improving the LEE and controlling the angular emission pattern [10]. These optical elements make the devices bulky and require extra steps in fabrication.

Recent progress in nanophotonics research has demonstrated that metasurfaces integrated with emitters can be a potential alternative of conventional optical elements for a new class of compact, integrated, and

high-performance devices [11–13]. Over the last two decades, researchers have investigated metasurfaces to enhance the light outcoupling and manipulate the emission direction from emitters [14–17]. The emission pattern can be modified by the interplay of resonant modes of the metasurfaces and can be engineered for particular applications that require beaming control [18–21]. This outcoupling enhancement and emission tailoring rely on the near-field coupling of the emitters and the resonant nanostructures, hence requiring the emitters to be placed at sub-wavelength distances from the metasurfaces [22, 23], which is not practical in commercial LED devices. In addition, researchers have tried to thin the n- or p-GaN cladding layer or etched through the active region of LEDs, (i.e. InGaN multiple quantum wells (MQWs)) to use the resonant nanostructures for steering the emission [24–28]. However, these approaches have a negative impact on the quality of the MQWs, resulting in an increase of non-radiative recombination processes that significantly reduce the emission efficiency. [29, 30].

In this article, we introduce an alternative approach to control the MQWs emission of blue LED wafers from a distance using plasmonic metasurfaces, which allows for avoiding the negative effect on the material properties and leads to a tailored far-field emission [22, 31]. Plasmonic metasurfaces can be made of a variety of materials that provide the possibility to cover the visible wavelength range, for example Al [16, 32], Au [33, 34], or Ag [35, 36]. Aluminum is an inexpensive metal that has low absorption losses in the blue range of the optical spectrum. We design arrays of Al with a resonant response at a wavelength close to the emission wavelength of blue LEDs, i.e. 440 nm. The fabricated arrays have different lattice constants ranging from 170 nm to 230 nm, with a step of 10 nm, and are at a distance of 110 nm away from the InGaN MQWs of the blue LEDs. The details on the fabrication can be found in the methods section. The integration of Al metasurfaces with commercial LEDs wafers introduces losses (metal absorption) in comparison with patterned sapphire substrates, which are used in commercial LED devices [37–40]. Nevertheless, these Al metasurfaces tailor the far-field emission from the blue LED wafer and enhance its intensity by outcoupling the trapped emitted light at angles larger than θ_c . This tailoring provides an opportunity for the beaming of the emission, which is needed for lighting applications such as head-mounted glasses for virtual reality or smartwatches based on mini- or micro-LEDs where patterning the substrate is not possible. In addition, the metasurfaces provide significant optical pump enhancement, although this pump enhancement will not be relevant in electrically driven devices. Power-dependent excitation measurements for the proposed Al metasurfaces designs allow an accurate determination of the light collection and pump enhancement.

2. Results and discussion

2.1. Description of the commercial blue emitting LED wafer integrated with Al metasurfaces

The system under study is schematically depicted in figure 1(a). The LED wafer consists of several layers including a thick 240 μm sapphire substrate, a 6 μm layer of GaN, two effective InGaN quantum wells with a total thickness of 10 nm, a 90 nm layer of p-GaN and a 20 nm layer of ITO. The proposed Al metasurfaces are on top of the ITO and are covered by a layer of Nb_2O_5 to obtain a homogeneous refractive index around the particles since the refractive index of GaN and Nb_2O_5 is 2.45 at 440 nm (for more details on the fabrication, see the Methods section). We show the measured photoluminescence (PL) emission spectrum of a LED wafer in figure 1(b). This PL was measured by exciting the MQWs with a continuous laser with $\lambda = 405$ nm and filtering the laser light. The PL emission exhibits a peak at the wavelength of 440 nm and has a bandwidth of around 20 nm, which is typical for blue LEDs. The metasurfaces were designed to tailor the MQWs emission and enhance the light extraction from the wafer at 440 nm.

2.2. Numerical simulations and their results

To determine the effect of metasurfaces on the emission from the MQWs, we perform numerical simulations based on the reciprocity principle using periodic boundary conditions (see methods) to calculate the far-field emission intensity $I(\theta, \phi)$ [41]. The intensity $I(\theta, \phi; \mathbf{r}_1)$ of the emission in the far-field along the direction (θ, ϕ) from a dipole source \mathbf{p}_1 positioned at \mathbf{r}_1 can be calculated as: [13, 42]

$$I(\theta, \phi; \mathbf{r}_1) \propto \int_0^{2\pi} \int_0^\pi \left[\sum_{TE, TM} |\mathbf{E}(\theta, \phi, \mathbf{r}_1) \cdot \mathbf{p}_1(\theta_p, \phi_p, \mathbf{r}_1)|^2 \right] \sin \theta_p d\theta_p d\phi_p, \quad (1)$$

where TE, TM denote the TE and TM polarizations of the plane wave incident on the structure along the direction (θ, ϕ) that produces the electric field $\mathbf{E}(\theta, \phi, \mathbf{r}_1)$ at the position of the source. The angles θ_p and ϕ_p define the orientation of the dipole source \mathbf{p}_1 , and the integration is performed to average over all possible orientations of this dipole. Since the orientation of the emitting dipoles affects the LEE, they are homogeneously distributed within the MQWs and their orientation distribution is on average 90% in-plane and 10% out-of-plane due to the geometry of the quantum wells.

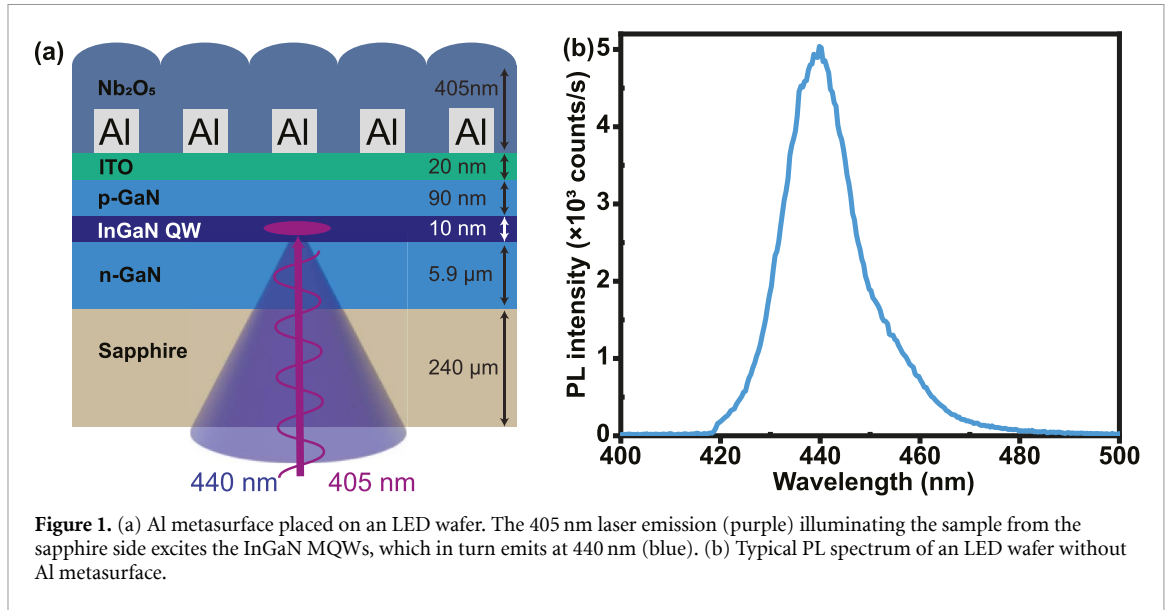


Figure 1. (a) Al metasurface placed on an LED wafer. The 405 nm laser emission (purple) illuminating the sample from the sapphire side excites the InGaN MQWs, which in turn emits at 440 nm (blue). (b) Typical PL spectrum of an LED wafer without Al metasurface.

Therefore assuming that $|\mathbf{p}_1| = 1$, equation (1) can be written as

$$I(\theta, \phi) \propto \sum_{TE, TM} \iiint_{MQWs} [0.45(|E_x(\theta, \phi, \mathbf{r}_1)|^2 + |E_y(\theta, \phi, \mathbf{r}_1)|^2) + 0.1|E_z(\theta, \phi, \mathbf{r}_1)|^2] d^3\mathbf{r}_1, \quad (2)$$

where the integration is performed over the volume occupied by the MQWs and the emission of the dipoles is considered incoherent. In this equation, we assume an isotropic in-plane distribution of incoherently emitting dipoles. From equation (2), the far-field emission intensity of the MQWs in a particular direction is directly proportional to the integrated electric field distribution in the MQWs' volume. Maximizing this electric field will lead to enhanced light extraction from a LED wafer. Consequently, we use a finite element method implemented in COMSOL to simulate the plane wave excitation of the structure and calculate the electric field distribution ($E_x(\mathbf{r}_1), E_y(\mathbf{r}_1), E_z(\mathbf{r}_1)$), so that we can estimate the emission intensity at the angles θ and ϕ using equation (2).

To match the simulated angles with the collection objective used in experiments (NA = 0.9), we have calculated the collection efficiency as we can not measure the total extraction efficiency, which requires a collection objective with NA = 1. Following equation (2), we optimized the parameters of the Al metasurfaces and the Nb₂O₅ thickness to maximize the integrated electric field distribution in the MQWs volume. During this optimization process, we found the parameters of the nanodisk to be a height of 55 nm and a diameter of 100 nm, the lattice constant of the array of 170 nm, and the Nb₂O₅ layer thickness of 405 nm. At a normal angle of incidence, we note that the variation of the Nb₂O₅ thickness introduces constructive or destructive interference at the MQWs position, as shown in the SI (figure S1). For the optimum lattice constant of 170 nm, the light collection enhancement factor is 2.4 with a pump enhancement of 1.5

To reconstruct the far-field emission pattern from the MQWs. We have performed far-field intensity calculations in the polar angle (θ) range from 0° to 63.6° and azimuthal angle (ϕ) range from 0° to 45° (angles are defined in air). Due to the four-fold and mirror symmetry of the lattice, these ranges are sufficient to reconstruct the emission pattern from the LED wafer. The results of our simulations are shown in figures 2(a)–(c), where each image is a map of the angle resolved far-field emission intensity $I(k_x, k_y)$, with $k_x = k_0 \sin\theta \sin\phi$ and $k_y = k_0 \sin\theta \cos\phi$, and k_0 is the wavevector in a vacuum. Despite the large distance (110 nm) between the MQWs and the metasurfaces, we observe a significant reshaping of the emission pattern compared to the reference which corresponds to the same sample, including the Nb₂O₅ layer but without metasurfaces.

This far-field tailoring of the emission originates from the scattering and diffraction from the MQWs emission with the Al nanodisks metasurfaces. As expected, we observe changes in the far-field emission for the metasurfaces with different lattice constants. The emitted blue light is scattered out of the LED following the grating equation [31].

$$\pm \mathbf{k}_d = \mathbf{k}_i + \mathbf{G}, \quad (3)$$

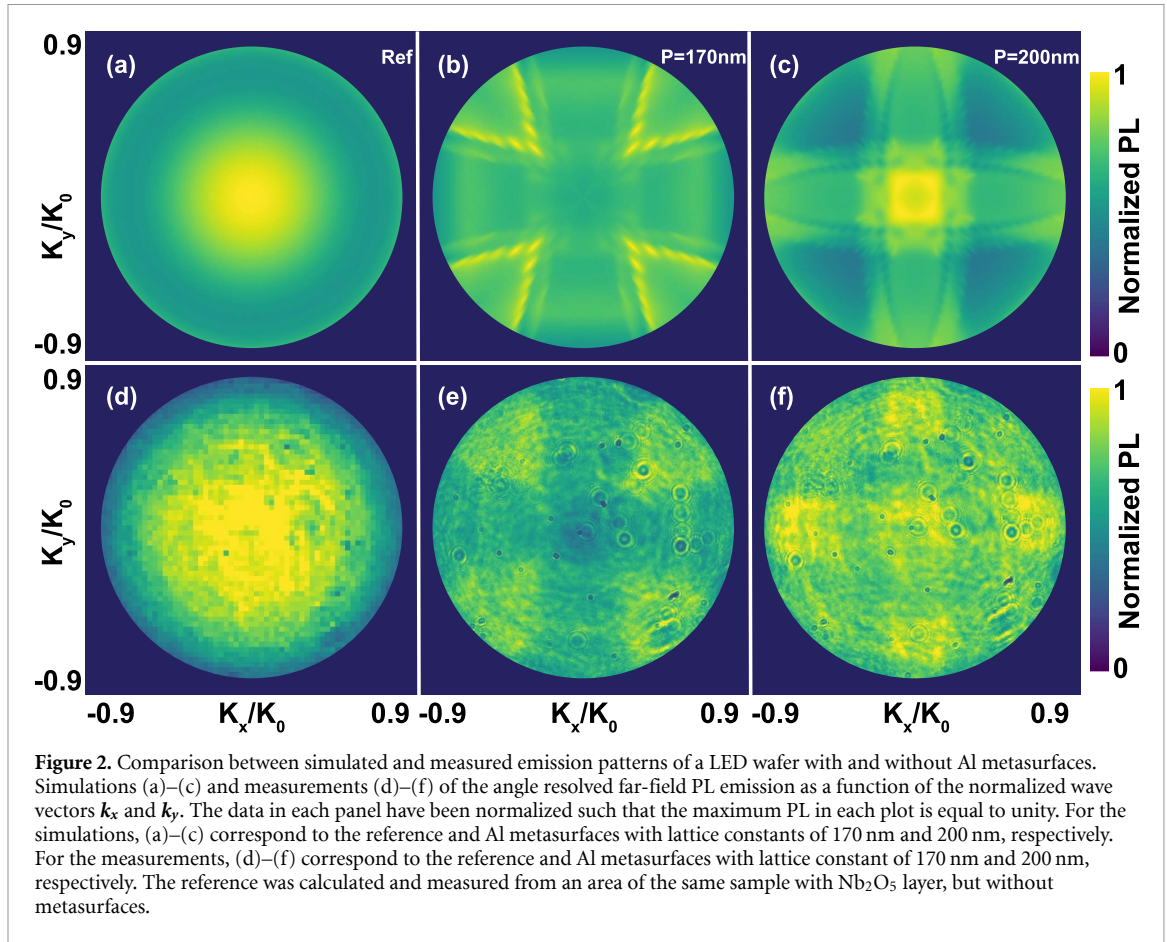


Figure 2. Comparison between simulated and measured emission patterns of a LED wafer with and without Al metasurfaces. Simulations (a)–(c) and measurements (d)–(f) of the angle resolved far-field PL emission as a function of the normalized wave vectors k_x and k_y . The data in each panel have been normalized such that the maximum PL in each plot is equal to unity. For the simulations, (a)–(c) correspond to the reference and Al metasurfaces with lattice constants of 170 nm and 200 nm, respectively. For the measurements, (d)–(f) correspond to the reference and Al metasurfaces with lattice constant of 170 nm and 200 nm, respectively. The reference was calculated and measured from an area of the same sample with Nb_2O_5 layer, but without metasurfaces.

where \mathbf{k}_d is the wave vector of the diffracted beam, \mathbf{k}_i is the wave vector of the incident beam, and \mathbf{G} is the reciprocal lattice vector of the Al grating ($\mathbf{G} = (\mathbf{G}_x, \mathbf{G}_y)$). \mathbf{G}_x is equal to \mathbf{G}_y for the square lattice, with $\mathbf{G} = (2\pi/a_x)p\mathbf{u}_x + (2\pi/a_y)q\mathbf{u}_y$ where (p, q) are integers giving the order of diffraction and (a_x, a_y) are the lattice constants. The far-field pattern in figure 2(b) shows the diffraction orders of $(0, \pm 1)$ and $(\pm 1, 0)$ represented by the vertical and horizontal parabolic lines, respectively.

By varying the lattice constant, the emitted blue light is reshaped to be emitted at different angles below θ_c , as shown in figures 2(b) and (c), respectively. This emission is calculated within the collection numerical aperture (NA) of the objective, which will be used in the experiment, and without taking into account the enhancement from the optical pump excitation at 405 nm. To determine the pump enhancement, we have also simulated the metasurface excited by a plane wave at 405 nm and calculated the electric field enhancement at the position of the MQWs. From these simulations, we have determined that the pump enhancement by the Al nanodisks array can reach a value of up to 3.3 while the LEE reaches a maximum value of 2.4 for the proposed square array.

2.3. Experimental results and analysis

To confirm the simulations, we have fabricated a sample with different Al nanodisk metasurfaces deposited onto a LED wafer and covered by a Nb_2O_5 layer, as shown in figure 1(a). In total, the sample has seven metasurfaces with different lattice constants ranging from 170 nm to 230 nm, with a step of 10 nm. A scanning electron microscope (SEM) image of a typical metasurface is shown in figure 3(a) before depositing the Nb_2O_5 layer. The SEM image in figure 3(b) corresponds to the surface of the wafer after depositing the Nb_2O_5 layer. Due to the shadowing effect during the sputter deposition process, the surface of the Nb_2O_5 is not flat. The details on the fabrication can be found in the methods section.

For the experiments, the excitation continuous wave (CW) laser emitting at the wavelength of 405 nm illuminated the InGaN MQWs from the sapphire side at normal incidence (see SI for the details on the experimental setup). The PL emission from the InGaN MQWs is collected by the objective through the sapphire and directed to the CCD camera or a spectrometer. We started the experimental investigation of the metasurface samples with the characterization of the angle resolved far-field emission by Fourier microscopy (as shown in the SI). In figures 2(d)–(f), we plot the measured Fourier images of the emission from the metasurfaces of different lattice constants (170 nm and 200 nm) and an empty area of the sample with the

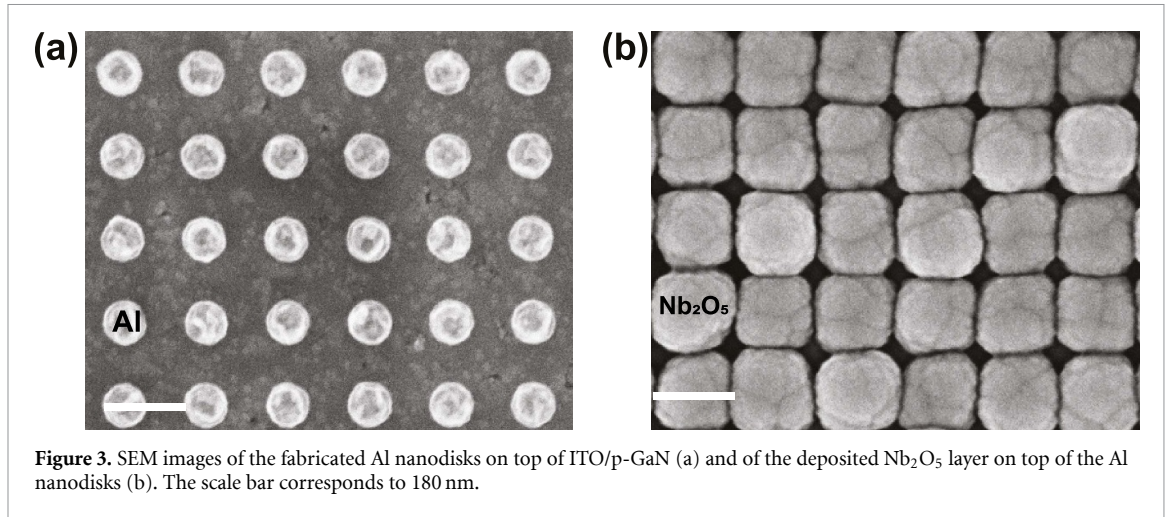


Figure 3. SEM images of the fabricated Al nanodisks on top of ITO/p-GaN (a) and of the deposited Nb₂O₅ layer on top of the Al nanodisks (b). The scale bar corresponds to 180 nm.

Nb₂O₅ layer but without metasurfaces for reference (figure 2(d)). Note that we used a 0.9NA collection objective and a bandpass filter with a center wavelength of 440 nm and full half width maximum (FWHM) of 10 nm in front of the CCD camera. The images are four-fold symmetric, which agrees with the symmetry of the metasurfaces and the simulations shown in figures 2(b) and (C). We obtain very similar emission patterns for the simulations (figures 2(b) and (C)) and the experiments (figures 2(e) and (f)).

To better characterize the pump and collection efficiencies, we have measured the excitation power dependent PL intensity from the metasurfaces. The Fourier images of the metasurfaces were taken for different powers of the excitation CW laser. The PL intensity at each excitation power was determined by the integration of the emission over all the pixels of the corresponding Fourier image. The power-dependent PL intensity measurements for the metasurfaces and the reference are shown in figure 4(a). Importantly, we observe that the PL intensity from the metasurfaces increases much faster with the pump power than the intensity from the reference. Overall, the PL from any of the metasurfaces is much larger compared to the reference, and the enhancement factor depends on the excitation power and lattices constant of the metasurface.

To explain this dependence, we analyze the carrier dynamics in the InGaN MQWs and how it is affected by a metasurface. Upon CW excitation, the carrier generation and recombination processes balance each other and the following equilibrium equation holds [43]:

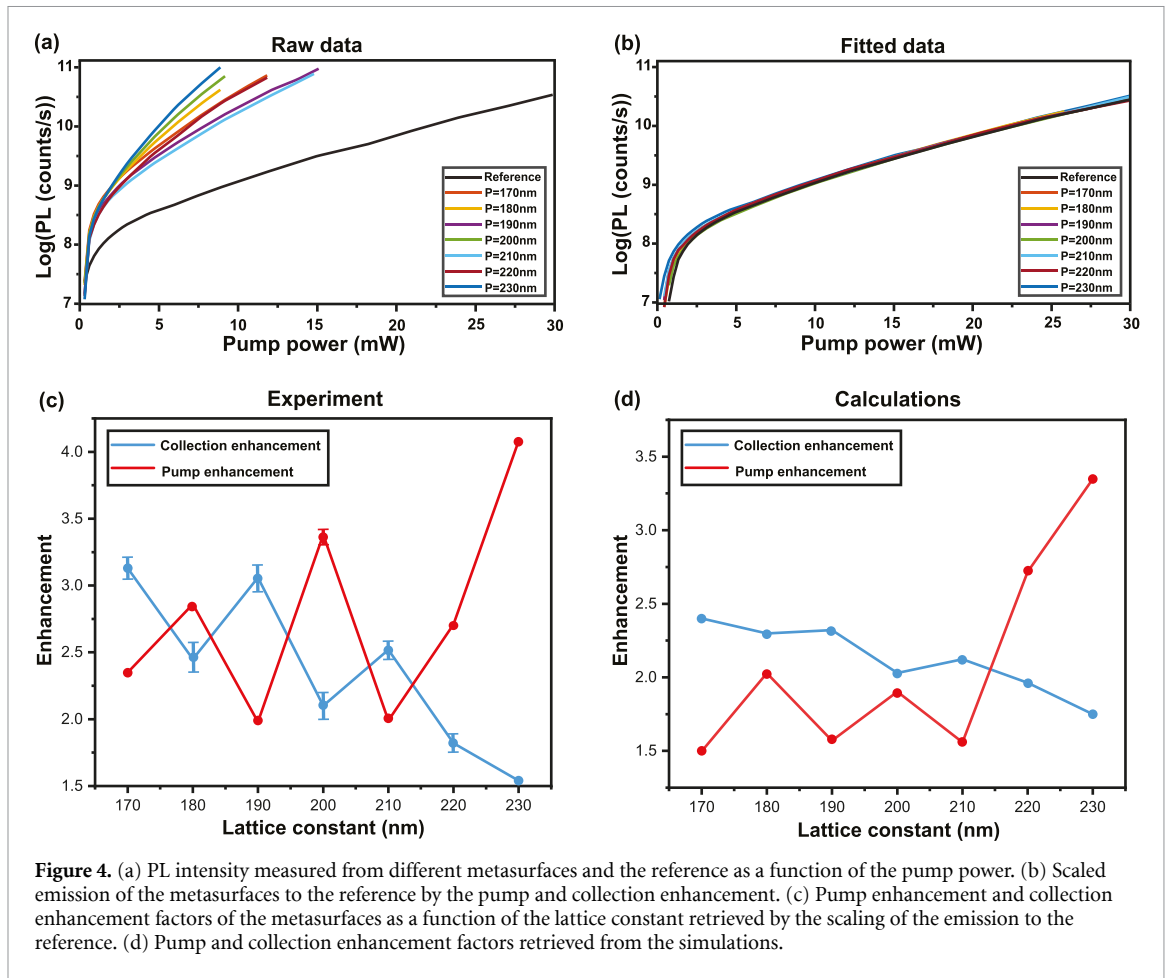
$$AN + BN^2 + CN^3 = a\alpha(N)W, \quad (4)$$

where the coefficients correspond to (A) Shockley–Reed–Hall recombination, (B) radiative recombination, and (C) Auger recombination. N is the photo excited carrier density, W is the power of the excitation laser beam and $\alpha(N)$ is the single-photon absorption coefficient of this laser beam ($\lambda = 405$ nm) by the InGaN MQWs. $\alpha(N)$ only depends on the solid-state properties of the GaN/InGaN alloy and the carrier concentration. We have introduced an additional coefficient a to describe the influence of a photonic environment on the absorption of the excitation laser. As described below, this coefficient accounts from the enhancement of the pump by scattering with the metasurfaces.

The PL emission intensity excited by the CW laser of power W is proportional to the radiative recombination and can be written as:

$$PL(aW) \propto BN(aW)b, \quad (5)$$

where b is the collection efficiency by the 0.9NA objective and after the bandpass filter with a center wavelength of 440 nm. Note that the shape of the PL spectrum does not change within the excitation power range used in our measurements, which is confirmed by figure S4 in the SI. The metasurfaces change the photonic environment and can affect the pump and emission processes. Indeed, at the excitation wavelength, a metasurface can scatter the laser light in a way that the incident and reflected waves interfere constructively at the position of the MQWs, thus exposing the MQWs to a higher intensity and providing a pump enhancement. Furthermore, as we demonstrated in figure 2, a metasurface can redirect the far-field emission toward the collection optics, which results in an improved collection efficiency. In general, a metasurface can also affect the radiative recombination coefficient B via the Purcell effect [44], but due to the lack of near-field coupling of the MQWs to the metasurfaces, this effect will be minor compared to the expected



changes in the pump and collection enhancement. Therefore, we neglect any change of the B coefficient by Purcell enhancement [22, 45].

The assumptions above suggest that the difference in the measurements depicted in figure 4(a) can be explained by the different pump and collection enhancement factors provided by the metasurfaces. We are able to estimate the relative values of these enhancement factors by fitting the experimental curve of the reference intensity to the measurements of the metasurfaces. According to equation (5), the pump enhancement (given by a) linearly scales the x -axis in figure 4(a), and the collection enhancement (given by b) linearly scales the measured PL counts under the logarithm in the y -axis of figure 4(a). To perform the fitting, we take the power dependent PL curve of a metasurface and perform a sweep over a certain range of different values of pump and collection enhancement factors. For each couple of values, we scale the reference power dependent PL curve and compare it with the metasurface curve. As an example, in figure S5 of the SI, we plot the inverse mean square error (MSE) of our fitting as a function of the pump and collection enhancement factors for a particular metasurface. This dependence of the inverse MSE on the enhancement factors exhibits a global maximum defining the optimal fitting values. Using this approach, we have estimated the optimal parameters for all the metasurfaces. In figure 4(b), we show the power dependent PL curves from all of the metasurfaces scaled in accordance with their corresponding pump and collection enhancements. We observe that all the scaled measurements overlap, which validates our assumptions.

The optimal pump and collection enhancement factors retrieved from the experimental measurements from all of the metasurfaces with different lattice constants are shown in figure 4(c). The plasmonic metasurfaces can provide a pump and a light collection enhancement factor of up to 4.1 and 3.2, respectively, where these values are relative to the pump and collection efficiency of the reference. Albeit the strong fluctuation of pump and collection enhancements, we observe an overall increase of the pump enhancement and a decrease of the collection enhancement with increasing the metasurface lattice constant. Figure 4(d) shows the light collection and pump enhancement retrieved from the simulations. In these curves, we observe the same qualitative dependence for the pump and collection enhancements.

3. Conclusion

To summarize, we have fabricated Al metasurfaces with different lattice constants on top of blue emitting wafers consisting of InGaN quantum wells for commercial LED devices to enhance the light collection efficiency and control the emission directionality. We have investigated the PL emission of the fabricated Al metasurfaces by varying the excitation power. From these power dependent measurements, we have determined the relative pump and light collection enhancement factors provided by the Al metasurfaces. A large collection enhancement factor of 3.2 is achieved with a simple square array of Al nanoparticles by reshaping the far-field emission. Fourier measurements of the emission from the metasurface samples show a reshaping of the far-field PL patterns, in agreement with simulations for the same lattice constants. Our findings suggest that Al metasurfaces can be integrated into commercial LEDs to improve the angle dependent emission and increase light outcoupling efficiency. This emission manipulation is essential for many lighting applications that require beaming such as the next generation of micro-LEDs where rough walls for enhanced light outcoupling are not possible due to their small dimensions. Importantly, our approach does not require the additional etching of the standard LED wafers to enhance the near-field coupling of the emission to the metallic nanoparticles. Therefore, this approach has no negative effect on the material quality and it could be integrated into commercial LEDs.

4. Methods

4.1. Finite element numerical simulation

A three-dimensional COMSOL model was set up for a unit cell with plane wave excitation and Floquet periodic boundary conditions on the horizontal edges and two ports (IN and OUT) on the vertical edges. The Floquet vector was defined by the corresponding wave vector projection of the incident plane wave. The TE- or TM- polarized plane wave was incident onto the metasurface from the p-GaN side along the (θ, ϕ) direction. We took into account that the dipoles are emitting on average 90% in-plane and 10% out-of-plane (1) as was indicated by the wafer manufacturer. We integrated the distributed field over the volume occupied by the MQWs to calculate the far-field emission. We used the experimental optical constants of the materials measured by ellipsometry (see SI).

4.2. Sample fabrication

The wafer used in this investigation was fabricated by Lumileds Holding B.V. The GaN/InGaN was grown using a metal-organic chemical vapor deposition reactor on a sapphire substrate followed by thinning the substrate to 240 μm . The wafer was covered and polishing the backside. The growth layers consist of 6 μm GaN, two effective InGaN/GaN quantum wells with a total thickness of 10 nm, and a p-GaN layer with a thickness of 90 nm. Details of this epitaxy technology and related materials are discussed in [46, 47]. The emission spectrum of the wafer is shown in figure 1(b). The wafer was covered by 20 nm of ITO using RF-magnetron sputtering deposition. Aluminum metasurfaces arrays were fabricated using electron beam lithography (EBL) and a lift-off process: the polymethyl methacrylate positive resist was coated onto the ITO with 240 nm thickness on the LED wafer and prebaked for 3 min at 135 $^{\circ}\text{C}$, followed by 4 min at 185 $^{\circ}\text{C}$. The positive resist was exposed using an EBL system (EBL, Raith EBPG 5150 100 kV) to nanopattern several nanodisks arrays with dimensions of 200 $\mu\text{m} \times 200 \mu\text{m}$ and varying the lattice constant from 170 nm to 230 nm, in steps of 10 nm. The resist was developed using MIBK/IPA 1:3 developer for 80 s. We used electron beam evaporation to evaporate 55 nm of Al and a lift-off process was performed using acetone to remove the resist covered by Al. Finally, we deposited a 405 nm of Nb_2O_5 using DC sputtering deposition. The fabricated Al metasurfaces were characterized before and after depositing Nb_2O_5 using atomic force microscopy (as shown in the SI) and scanning electron microscopy.

4.3. Fourier microscopy measurements

We measured the angle resolved PL emission from the LED wafer with and without Al metasurfaces using Fourier microscopy. We optically pumped the sample using a CW laser at a wavelength of 405 nm. The PL was collected by 0.9NA Nikon Plan Fluor 100 \times and the residual laser light was filtered out by a 405 nm notch filter followed by a bandpass filter with FWHM of ~ 10 nm to selectively map the PL within a narrow spectral region. The angle resolved PL was measured with a CMOS camera (Andor Neo 5.5).

Data availability statement

The datasets used and/or analyzed during the current study are available from the corresponding author upon reasonable request. The data that support the findings of this study are available upon reasonable request from the authors.

Acknowledgments

This work has been financially supported by the Nederlandse Organisatie voor Wetenschappelijk Onderzoek (NWO), domain Applied and Engineering Sciences (TTW), through Grant no 17100 (NanoLEDs). The authors thank Casper F Schippers for helping to optimize the deposition parameters of Aluminum using an electron beam evaporator.

Conflict of interest

The authors declare no conflicts of interest.

ORCID iD

Mohamed S Abdelkhalik  <https://orcid.org/0000-0003-3963-3481>

References

- [1] Nanishi Y 2014 *Nat. Photon.* **8** 884–6
- [2] Wu T, Sher C W, Lin Y, Lee C F, Liang S, Lu Y, Huang Chen S W, Guo W, Kuo H C and Chen Z 2018 *Appl. Sci.* **8** 1557
- [3] Taki T and Strassburg M 2019 *ECS J. Solid State Sci. Technol.* **9** 015017
- [4] Huang Y, Tan G, Gou F, Li M C, Lee S L and Wu S T 2019 *J. Soc. Inf. Disp.* **27** 387–401
- [5] Xiong J, Hsiang E L, He Z, Zhan T and Wu S T 2021 *Light Sci. Appl.* **10** 216
- [6] Raju G S R, Lee H K, Yu J S and Ko Y H 2012 *Opt. Express* **20** 25058–63
- [7] Dang S, Li C, Li T, Jia W, Han P and Xu B 2014 *Optik* **125** 3623–7
- [8] Zhmakin A I 2011 *Phys. Rep.* **498** 189–241
- [9] Gu X, Qiu T, Zhang W and Chu P K 2011 *Nanoscale Res. Lett.* **6** 1–12
- [10] Khanh T 2015 *LED Lighting : Technology and Perception* (Weinheim: Wiley-VCH)
- [11] Pfeiffer C and Grbic A 2013 *Phys. Rev. Lett.* **110** 197401
- [12] Lozano G, Grzela G, Verschuuren M A, Ramezani M and Rivas J G 2014 *Nanoscale* **6** 9223–9
- [13] Vaskin A, Kolkowski R, Koenderink A F and Staude I 2019 *Nanophotonics* **8** 1151–98
- [14] Okamoto K, Niki I, Shvartser A, Narukawa Y, Mukai T and Scherer A 2004 *Nat. Mater.* **3** 601–5
- [15] Hancu I M, Curto A G, Castro-López M, Kuttge M and Hulst N F V 2014 *Nano Lett.* **14** 166–71
- [16] Lozano G, Rodriguez S R, Verschuuren M A and Rivas J G 2016 *Light: Sci. Appl.* **5** e16080
- [17] Mota A F, Martins A, Ottevaere H, Meulebroeck W, Martins E R, Weiner J, Teixeira F L and Borges B H V 2018 *ACS Photonics* **5** 1951–9
- [18] Langguth L, Punj D, Wenger J and Koenderink A F 2013 *ACS Nano* **7** 8840–8
- [19] Lozano G, Grzela G, Verschuuren M A, Ramezani M and Rivas J G 2014 *Nanoscale* **6** 9223–9
- [20] Langguth L, Schokker A H, Guo K and Koenderink A F 2015 *Phys. Rev. B* **92** 205401
- [21] Vaskin A, Bohn J, Chong K E, Bucher T, Zilk M, Choi D Y, Neshev D N, Kivshar Y S, Pertsch T and Staude I 2018 *ACS Photonics* **5** 1359–64
- [22] Novotny L and Hecht B 2012 *Principles of Nano-Optics* (Cambridge: Cambridge University Press)
- [23] Koenderink A F 2017 *ACS Photonics* **4** 710–22
- [24] Wierer J J, Krames M R, Epler J E, Gardner N F, Craford M G, Wendt J R, Simmons J A and Sigalas M M 2004 *Appl. Phys. Lett.* **84** 3885–7
- [25] Henson J, Dimakis E, DiMaria J, Li R, Minissale S, Negro L D, Moustakas T D and Paiella R 2010 *Opt. Express* **18** 21322–9
- [26] Galfsky T, Gu J, Narimanov E E and Menon V M 2017 *Proc. Natl Acad. Sci.* **114** 5125–9
- [27] Shen K C, Hsieh C, Cheng Y J and Tsai D P 2018 *Nano Energy* **45** 353–8
- [28] Iyer P P, DeCrescent R A, Mohtashami Y, Lheureux G, Butakov N A, Alhassan A, Weisbuch C, Nakamura S, DenBaars S P and Schuller J A 2020 *Nat. Photon.* **14** 543–8
- [29] Yu Z G et al 2012 *Chin. Phys. Lett.* **29** 078501
- [30] Polyakov A, Alexanyan L, Skorikov M, Chernykh A, Shchemerov I, Murashev V, Kim T H, Lee I H and Pearton S 2021 *J. Alloys Compd.* **868** 159211
- [31] Wierer J J, David A and Megens M M 2009 *Nat. Photon.* **3** 163–9
- [32] Knight M W, Liu L, Wang Y, Brown L, Mukherjee S, King N S, Everitt H O, Nordlander P and Halas N J 2012 *Nano Lett.* **12** 6000–4
- [33] Muskens O L, Giannini V, Sánchez-Gil J A and Rivas J G 2007 *Nano Lett.* **7** 2871–5
- [34] Sung J H, Kim B S, Choi C H, Lee M W, Lee S G, Park S G, Lee E H and Beom-Hoan O 2009 *Microelectron. Eng.* **86** 1120–3
- [35] Khurgin J B, Sun G and Soref R A 2008 *Appl. Phys. Lett.* **93** 021120
- [36] Akselrod G M, Argyropoulos C, Hoang T B, Ciraci C, Fang C, Huang J, Smith D R and Mikkelsen M H 2014 *Nat. Photon.* **8** 835–40
- [37] Wu D S, Wang W K, Shih W C, Horng R H, Lee C E, Lin W Y and Fang J S 2005 *IEEE Photonics Technol. Lett.* **17** 288–90
- [38] Wu D S, Wang W K, Wen K S, Huang S C, Lin S H, Huang S Y, Lin C F and Horng R H 2006 *Appl. Phys. Lett.* **89** 161105
- [39] Li G, Wang W, Yang W, Lin Y, Wang H, Lin Z and Zhou S 2016 Gan-based light-emitting diodes on various substrates: a critical review *Rep. Prog. Phys.* **79** 056501

- [40] Wang K, Tian Y, Li M, Zhang H, Chen Z, Wei Y and Yu T 2021 *ACS Appl. Electron. Mater.* **3** 4905–11
- [41] Landau L D, Lifshitz E M and King A L 1961 *Am. J. Phys.* **29** 647–8
- [42] Zhang S, Martins E R, Diyaf A G, Wilson J I, Turnbull G A and Samuel I D 2015 *Synth. Met.* **205** 127–33
- [43] Schubert E F 2012 *Light-Emitting Diodes* 2nd edn (Cambridge: Cambridge University Press)
- [44] Purcell E M 1946 Spontaneous emission probabilities at radio frequencies *Phys. Rev.* **69** 681
- [45] Drexhage K 1970 *J. Lumin.* **1–2** 693–701
- [46] Wildeson I 2017 Improved ingan led system efficacy and cost via droop reduction *Technical Report* (San Jose, CA: Lumileds LLC)
- [47] Lee K 2022 solid-state lighting R&D opportunities *Technical Report* (Guidehouse)